Design and evaluation of an abbreviated pixelwise dynamic contrast enhancement analysis protocol for early extracellular volume fraction estimation

J.S. Louis, F. Odille, D. Mandry, Christian de Chillou, O. Huttin, J. Felblinger, C. Venner, M. Beaumont

DESIGN AND EVALUATION OF AN ABBREVIATED PIXELWISE DYNAMIC CONTRAST ENHANCEMENT ANALYSIS PROTOCOL FOR EARLY EXTRACELLULAR VOLUME FRACTION ESTIMATION

J.S. Louis[1], F. Odille[1, 2], D. Mandry[1, 3], C. De Chillou[1,4], O. Huttin[4], J. Felblinger[1, 2, 3], C. Venner[4], M. Beaumont[1,2]

[1] Université de Lorraine,IADI, INSERM U1254, Nancy, France;
[2]CIC-IT, INSERM 1433, Université de Lorraine and CHRU Nancy, Nancy, France;
[3]Pôle Imagerie, CHRU Nancy, Nancy, France;
[4]Pôle Cardiologie, CHRU Nancy, Nancy, France.

Jean-Sébastien Louis* ..... jean-sebastien.louis@inserm.fr
Freddy Odille ..... freddy.odille@inserm.fr
Damien Mandry ..... d.mandry@chru-nancy.fr
Christian De Chillou ..... c.dechillou@chru-nancy.fr
Olivier Huttin ..... o.huttin@chru-nancy.fr
Jacques Felblinger ..... j.felblinger@chru-nancy.fr
Clément Venner ..... clemvenner@gmail.com
Marine Beaumont ..... m.beaumont@chru-nancy.fr

* : Corresponding author

Common adress :
Bâtiment Recherche, Rez-de-Chaussée
CHRU de Nancy Brabois
Rue du Morvan
54511 VANDOEUVRE-LES-NANCY
Tél : +33.3.83.15.78.23

DESIGN AND EVALUATION OF AN ABBREVIATED PIXELWISE DYNAMIC CONTRAST ENHANCEMENT ANALYSIS PROTOCOL FOR EARLY EXTRACELLULAR VOLUME FRACTION ESTIMATION

ABSTRACT:

Introduction

T1-based method is considered as the gold standard for extracellular volume fraction (ECV) mapping. This technique requires at least a 10 minutes delay after injection to acquire the post injection T1 map. Quantitative analysis of Dynamic Contrast Enhancement (DCE) images could lead to an earlier estimation of an ECV like parameter (2 minutes). The purpose of this study was to design a quantitative pixel-wise DCE analysis workflow to assess the feasibility of an early estimation of ECV.

Methods

Fourteen patients with mitral valve prolapse were included in this study. The MR protocol, performed on a 3T MR scanner, included MOLLI sequences for T1 maps acquisition and a standard SR-turboFlash sequence for dynamic acquisition. DCE data were acquired for at least 120s. We implemented a full DCE analysis pipeline with a pre-processing step using an innovative motion correction algorithm (RC-REG algorithm) and a post-processing step using the extended Tofts Model (ECV_{ETM}). Estimated ECV_{ETM} maps were compared to standard T1-based ECV maps (ECV_{T1}) with both a Pearson correlation analysis and a group-wise analysis.

Results

Image and map quality assessment showed systematic improvements using the proposed workflow. Strong correlation was found between ECV_{ETM}, and ECV_{T1} values (r-square=0.87).

Conclusion

A DCE analysis workflow based on RC-REG algorithm and ETM analysis can provide good quality parametric maps. Therefore, it is possible to extract ECV values from a 2 minute-long DCE acquisition that are strongly correlated with ECV values from the T1 based method.

KEYWORDS: Cardiac MR; DCE-MRI; REGISTRATION; PERMEABILITY; ECV

Manuscript:

1 INTRODUCTION :

Myocardial extracellular volume (ECV) is considered as a key biomarker for the quantification of myocardial fibrosis using magnetic resonance imaging (MRI) [1], [2]. It was first qualitatively studied on local infarcted area with the so-called late gadolinium enhancement or delayed enhancement technique [3], which is based on the signal enhancement observed in the myocardium few minutes (15-20 minutes i.e. at the equilibrium of concentrations between compartments) after the injection of a paramagnetic contrast agent (CA) distributing within the extracellular extravascular space (EES) [4]. The accumulation of contrast agent within large EES, such as in infarcted tissues, leads to a brighter signal on T1-weighted (T1w) images than on the healthy myocardium [5]. Quantitative assessment of ECV has been lately developed using T1 measurements before injection and once the equilibrium state of CA concentrations between vascular space and EES has been reached [6]. This technique is well-known and denoted as ECV mapping. The very straightforward formula and its ease of use (as long as specific cardiac T1 mapping sequences are available) made it remarkably popular in the last few years and yield very promising results for diffuse fibrosis diagnosis [1], [7]. However, the major disadvantage of this technique lies in its duration, with a required long waiting time before reaching the steady-state concentration between injection and acquisition of the post-injection T1 map (>10 minutes according to the latest statement of the SCMR community [8]). Cardiac MRI (CMR) exams are among the longest MRI exams and there is a crucial need to shorten the total duration of CMR exam. Several options have been investigated in order to assess myocardial tissue pathophysiological state in a shorter time. Non-contrast enhanced imaging with diffusion weighted imaging (DWI) has

been investigated for more than a decade [9]. However, despite its huge potential, cardiac DWI is very complex to set up and improvements are still required before its use in clinical routine with a high reproducibility[10]. Another avenue of research consists in taking advantage of T1w Dynamic Contrast Enhanced (DCE) acquisition, which could bring early and new insights on the myocardium viability. From the early works of Wilke et al.[11] and Jerosch-Herold et al. [12] to the latest works of Knot et al. [13] using fully automatic in-line perfusion analysis [14], myocardial perfusion quantification has been mostly focusing on myocardial blood flow estimation from the first-pass analysis of the CA injection. Several models have been explored to quantify the myocardial blood flow; but constraint Fermi deconvolution [12] or Blood Tissue Exchange Model [15] remain the most studied to this day. Bi-compartmental models like the Extended Tofts Model (ETM) based on the Kety model have also been investigated with various conclusions regarding the impact on myocardial viability assessment [16]. Larsson et al.[17] showed that the extracellular extravascular volume fraction Ve extracted from pharmacokinetic models could be a good predictive factor of the interstitial volume, which is also quantified with the ECV method. A little bit more than a decade ago, Pack et al. [18] investigated the relationship between the compartmental parameter Ve and the so called "*steady-state*" tissue enhancement method. They demonstrated a non-significant difference between these two parameters. However, they could not compare their results to ECV extracted from T1 maps largely validated against histology. More recently, Kunze and colleagues compared measurements of ECV using the T1 maps method (equilibrium ECV) with the ECV extracted from perfusion quantification (perfusion ECV) [19]. They demonstrated a good correlation between ECV values extracted from both methods. They used a hierarchical modeling approach to estimate ECV

from perfusion data using up to 5 parameter-models. This approach did not include standard permeability model such the 3 parameter-ETM.

The present work aims to pursue these investigations by comparing ECV values obtained from T1 maps (ECV_{T1}) with those derived from parameters of the ETM analysis of perfusion imaging (ECV_{ETM}).

The first step in the development of a full DCE analysis pipeline was to implement a motion correction algorithm for images acquired in free breathing. This step presented a critical challenge due to the joint presence of contrast variation and respiratory and cardiac motion . Our vendor-provided in-line motion correction algorithm, MOCO [20], aligns each image of the series to the previous one. It is known to be prone to registration error propagation and to eventually introduce distortion in registered images, especially when acquisition time exceeds first-pass (about 1min) [20]. Thus, myocardial first-pass DCE registration has been and is still extensively investigated using various strategies such model-based registration [21], independent component analysis [22] or using robust large displacement optical flow [23]. This problem was already assessed in DCE studies on other organs. For instance, Hamy et al. used a robust Principal Component Analysis to register DCE data from bowel [24] employing a similarity indicator robust to intensity variation called residual complexity (RC) [25]. We hypothesized that such similarity indicator could also be a suitable solution to myocardial DCE registration.

Thereby, the goal of this study was two-fold. First, it aimed to assess our proposed registration algorithm compared to the vendor's in-line registration algorithm MOCO. Second, it aimed to investigate the feasibility of an early ECV estimation from 2min-

long DCE-MRI analyzed with the Extended Tofts Model compared to the regular 10min ECV estimation from the T1 mapping method.

2 MATERIALS AND METHODS:

2.1 Acquisition of DCE data and T1 maps

MR data of 14 patients, with suspected or diagnosed mitral valve prolapse were extracted from the STAMP (STretch and Myocardial Characterization in Arrhythmogenic Mitral Valve Prolapse) study (NCT02879825), and were analyzed for the purpose of this study. STAMP was approved by the local committee of ethics, wherein all participants provided written informed consent. Every patient had a single measure of hematocrit (hct) that was used for ECV calculation. The CMR protocol was performed on a 3Tesla (T) MR scanner (Prisma, Siemens Healthineers, Erlangen, Germany).

Injection consisted in a 0.15mmol/kg bolus Gd-DOTA (Dotarem®, Guerbet, France) at least 6 seconds after the beginning of the dynamic acquisition at a rate of 4mL/s. The pre-bolus T1 map ($T1_0$ map) was acquired with a single shot MOLLI set of 8 TI samples (5(3)3) on 8 slices covering the heart from the left atrium to the mid ventricular area (TR/TE: 283/1.12ms, matrix: 256x220, in plane resolution: 1.40x1.40mm², Slice Thickness: 8mm). DCE series lasted for at least 116 seconds in free breathing or partial free-breathing using a SR-TurboFLASH sequence (TI: 95ms, TR/TE: 116/0.97ms, flip angle:10°, matrix: 160x116, in plane resolution: 2.25x2.25mm², slice thickness: 8mm). The acquisition was cardiac gated meaning temporal resolution varied (mean: 0.95±0.13s) depending on the patient's heart rate. To ensure a temporal resolution equal to one RR-interval, the maximum number of slices was defined by the acquisition time available within one RR interval. This resulted in the acquisition of one to two slices maximum par RR interval. Post-T1 map was acquired with a single shot MOLLI sequence set of 9 TI samples for 4(1)3(1)2 at least 15 minutes after the injection $T1_0$ map, DCE series and post-

T1map slices were set to be automatically acquired at the same location with the same orientation and extra care was taken to ensure the acquisitions were performed during the same cardiac phases.

2.2 ECV mapping using extended Tofts modelling

The processing pipeline of this study (Figure 1) was implemented in Matlab® (The Mathworks, Natick,MA, USA).

The first step consisted in the registration of the magnitude images of the DCE series using our homemade registration algorithm (RC-REG). DCE acquisitions were normalized using a pre-scan calibration in order to attenuate signal inhomogeneity from the coil profile across the slice. The specific difficulty met with DCE images registration is the contrast change from one image to another, especially during the bolus arrival. The originality of this registration algorithm was the use of two reference images for the successive registration of pre-bolus and post-bolus acquisitions. Registration of DCE images was based on a 2-dimensional non-rigid algorithm using b-spline deformation model with gradient descend optimization using the residual complexity (RC) as similarity measure included in the Medical Image Registration Toolbox developed by Myronenko et al. [25]. RC-REG algorithm is further described in Figure 2.

The algorithm was set to iterate until both the mean and standard deviation (SD) of the Structure Similarity (SSIM) [26] scores of the registered DCE series reached empirically determined cutoff values (mean > 0.81 and std < 0.028). Thus, the algorithm kept iterating using the newly registered DCE images as a starting point. This allowed the algorithm to manage DCE series with large respiratory motion, which leads to blurry averaged DCE series after the first iteration.

The $T1_0$ map was resized and downsampled to fit the DCE series resolution and FoV. Then, $T1_0$ map was aligned to the registered DCE series averaged image using the Matlab® multimodal 2-dimensional rigid registration algorithm (function imregister). A pixel-wise signal to CA concentration conversion on the DCE series was then performed.

To shorten post-processing, automatic cropping was applied to all DCE images. First, the region of interest was selected based on both the maximum intensity of the DCE series and shape segmentation of the Left Ventricle (LV) chamber. Then, the coordinates of a rectangle were calculated to widen the region of interest area and to prevent over cropping. The resulting cropping was applied to the corresponding $T1_0$ map. Registration quality measurements were evaluated on this area of interest.

DCE signals were interpolated using a piecewise cubic Hermite interpolation algorithm to a constant temporal resolution of 0.5s.

AIF was measured for each exam. Since it has been shown that RC algorithm does not alter signal of the corrected image [24], [25], we considered that sampling the AIF from the RC-REG series was the best solution to extract reliable signal intensity dynamics of the vascular space without being polluted by motion. A manual region of interest (ROI) was placed in the center of LV cavity to extract blood signal intensity dynamics.

Pixel-wise dynamic T1 values were processed from (pixel-wise) normalized signal intensity curves associated with baseline signal mean value, i.e. before injection (acquired for at least 6 seconds), and corresponding $T1_0$ voxel value using the signal equation of the SR-turboFLASH sequence. Ultimately, CA concentration was

calculated for each pixel using the linear relationship between T1 and CA concentration:

$$\frac{1}{T1_{i,j,k}} = r \cdot [CA]_{i,j,k} + \frac{1}{T1_{0\ i,j}}, \quad (2)$$

with i,j the coordinates of the pixel of interest, k the time, $T1_{i,j,k}$ the T1 value; r the relaxivity of the CA at 3T, 3.6 $mM^{-1}.s^{-1}$, $[CA]_{i,j,k}$ the CA concentration and $T1_{0\ i,j}$ the T1 extracted from $T1_0$map.

Extended Tofts modeling was achieved using a trust region least square algorithm generating Ktrans, Kep the flux rate parameters and Vb the blood volume fraction maps using the following formula:

$$Ct(t) = Cb(t) * K_{trans} \cdot\ e^{-K_{ep} \cdot t} + Cb(t) \cdot Vb, \quad (3)$$

with Ct, the tissue concentration and Cb the blood concentration. Ve' maps were calculated using the relation Ve' = Ktrans/Kep. Before fitting, AIF was temporally shifted to adjust the bolus arrival time to the one of the dynamic tissue concentration curve Ct(t) by computing cross-correlation between the two curves. Extracellular extravascular volume fraction Ve was calculated by correcting Ve' with each subject's hematocrit (hct) so that: Ve = Ve' · (1-hct). Likewise, plasma volume fraction was computed such as Vp = Vb · (1-hct). ECV corresponds to the non-cellular volume fraction of a tissue[1], [27], and therefore to the EES plus the plasma volume fraction. We calculated the ECV values from ETM analysis so that ECV_{ETM} = Ve+Vp. ECV_{T1} were computed using the classical T1 maps technique and individual hct values [7]. Native and post blood T1 were measured within a ROI manually drawn in the center of the LV cavity. Full size native and post T1 maps were registered with the same

multimodal 2D rigid registration algorithm used to register the $T1_0$ map and the mean DCE series. ECV maps were computed with the following formula:

$$ECV_{T1(i,j)} = (1 - hct) \cdot \frac{\left(R1^{post}_{myo_{(i,j)}} - R1^{native}_{myo\ (i,j)}\right)}{\left(R1^{post}_{blood} - R1^{native}_{blood}\right)},$$

where $R1^{post/native}_{myo/blood}$ correspond to post/native 1/T1 of the myocardial/blood.

2.3 Evaluation of the motion correction and permeability maps

The registration algorithm was qualitatively assessed by extracting dynamic line profiles of DCE series. Two line-profiles were extracted for each DCE series. Line profiles from unregistered (UNREG), in-line MOCO algorithm (MOCO) and RC-REG series were compared. Registration quality of the proposed algorithm was also assessed on permeability maps, looking at the absence of abnormal deformation of the LV. Also, homogeneous and/or a less “noisy” map was considered of a global higher quality.

Permeability parameter measurement was achieved within ROI manually drawn around the endocardium and epicardium of the LV and divided into the regular AHA (American Heart Association) segments [28] on one to two slices per subject (from basal to medial level). Because slices were basal to medial, we concatenated segments from these slices into a single segment value to finally extract 6 segment values per subject. Permeability measurements were performed only when the thickness of the whole myocardium wall was sufficient to avoid any partial volume effect.

2.4 Comparison between ECV_{ETM} and ECV_{T1}

Diffuse fibrosis is a process at the root of several cardiomyopathies and is not restricted to a specific location but that affects the whole myocardium. Therefore, we considered the global myocardial mean value of ECV_{ETM} and ECV_{T1} as representative of the general state of fibrosis infiltration. For each patient, we therefore calculated the ECV median± median absolute deviation (mad) values from the measured segments.

Pearson correlation with a significance level of 0.05 was used to compare ECV_{ETM} from the three series and ECV $_{T1}$ myocardial values for the three series: UNREG, MOCO and RC-REG.

We chose to evaluate the discrimination power of ECV_{ETM} versus ECV_{T1} as follows: an ECV_{T1}value higher than 0.30 was considered as abnormal, splitting the patients into two groups. We then evaluated the difference between the two groups of ECV_{T1} and associated ECV_{ETM} values with a permutation test.

3 RESULTS:

3.1 Evaluation of the motion correction and permeability maps

Line profiles inspection of the fourteen exams showed, except for a few exceptions mentioned later, that respiratory motion correction was possible with MOCO and RC-REG algorithms (i.e. respiratory patterns were smoothened). Figure 3 provides two examples of typical line profiles with two different orientations obtained from UNREG, MOCO and RC-REG series. One can observe that MOCO registration introduced image distortions after the first-pass period on every exam, which never occurred with the RC-REG algorithm. These registrations are available in supplementary materials where the deformations of the LV on MOCO series can clearly be seen.

It has to be noted that DCE series from exam 11, which showed very large respiratory movements, was neither properly registered by MOCO nor the RC-REG algorithm.

Figure 4 shows two examples of ETM permeability maps. Visual assessment of permeability maps indicates that maps computed from MOCO DCE series were also highly impacted by the deformation generated during registration process. Maps extracted from UNREG DCE series appeared to be affected at different levels by respiratory motion, especially on inferior segments, which exhibited heterogeneous values for each permeability parameter. RC-REG permeability maps showed more homogeneous permeability parameter values over the left ventricle than permeability maps with other registration techniques.

Two exams had to be discarded from the analysis because the myocardium thickness (<2 pxls) did not allow an ROI to be placed without including voxels affected by partial volume effect.

3.2 Comparison between ECV_{ETM} and ECV_{T1}

Figure 5 highlights the excellent correlation between ECV_{ETM} and ECV_{T1}values (r-square=0.87) with a unity slope but a slight offset (= -0.05).

As shown in Figure 6, the 12 exams were split into two small groups of unequal size (n=8 for ECV≤0.30 and n=4 for ECV> 0.30). For both ECV methods, permutation test gave a statistically significant mean difference between the two groups. Boxplot analysis indicated a clear differentiation between the two groups of ECV_{ETM} series with no overlapping of the upper and lower whiskers (lower group ECV>0.30 corresponded to ECV_{ETM}=0.22; upper group ECV<0.30 corresponded to ECV_{ETM}=0.20) which was naturally also the case for ECV_{T1} subgroups (lower group ECV>0.30 corresponded to 0.32; upper group ECV<0.30 corresponded to 0.28) which was our reference.

4 DISCUSSION:

4.1 Evaluation of the motion correction and permeability maps

In order to proceed to ECV_{ETM} evaluation, we first proposed a novel DCE imaging registration algorithm. This algorithm used RC as a similarity indicator between two images. Well known in the post-processing community [29], residual complexity has been used in few MRI studies and mostly for abdominal exams [24], [30], [31]. It is only very recently that Scannell et al. used RC as a similarity indicator integrated in a Robust principal component analysis (RPCA) based registration algorithm for first pass perfusion imaging [32]. Compared to the latter work, our algorithm is based on an iterative optimization process of 2 similarity indicators (SSIM and RC), which could improve the quality of the registration compared to a two-step registration process. In this study, we also demonstrated the feasibility to register perfusion data from longer acquisition than what was assessed previously. Furthermore, the impact of the proposed registration algorithm was evaluated on both native DCE data and permeability maps.

Results of our study confirmed that RC-based algorithms offer better registration for free-breathing DCE cardiac MRI images than the vendor's in-line MOCO in terms of line profiles (figure 3), and permeability maps quality (figure 4). MOCO is well known to incrementally introduce distortions on the corrected images as the processed image is further away from the bolus arrival in the LV. This phenomenon is well described in literature [20], [33], [34] and can be observed in figure 3 and supplementary videos.

RC-REG is a 2D registration algorithm (like MOCO), which implies that it is intrinsically unable to register through-plane motion leading to lower similarity metric

scores from one image to another. It is also a post-processing algorithm and therefore dependent on the quality of the ECG gating during the prospective image acquisition. This acquisition technique is known to be sensitive to irregular heart rates [35], [36] and even if DCE images were correctly aligned, the apparent thickness of the left ventricle may vary if such mistriggered data are present. This issue was not address in this work but it is visible on supplementary material 1. Such isolated mistriggered acquisitions could be potentially discarded from the DCE dataset and replaced using temporal interpolation with very low impact on the final analysis. However, several consecutive acquisitions at wrong cardiac phases during the bolus arrival might lead to strongly biased parameter estimation, which was not encountered during this study. Despite these common limitations (shared between MOCO and other registration algorithms) our solution demonstrated better results both qualitatively and quantitatively compared to MOCO. It also showed comparable results compared to other more complex algorithms proposed in the literature [23], [32], [37].

Two exams were acquired in a partial free-breathing paradigm, i.e. the patient was asked to hold his/her breath as long as possible [35]. The reference image for post-injection data was found to be in a very different location from the reference image for pre-injection data for these patients. Our registration technique did not fully overcome this limitation resulting in a slight shift of the data particularly visible in the right ventricle (figure 3.B). Nonetheless, it had no visible impact on the processed permeability maps. It has to be noted that the registration between reference 1 (from baseline series) and reference 2 (from entire series), resulting images would also be inadequate in the case of poor cardiac triggering between the baseline acquisition and the acquisition after the bolus arrival. The non-rigid nature of this deformation

would lead to incomplete registration of those two images and would end as being discarded in the study. The use of a non-rigid registration for the alignment of these two reference images would be an interesting avenue of research, although it would not guarantee that the aligned pixels would coincide with a real volume alignment because of the complex nature of cardiac fibers motion between cardiac phases.

Permeability maps from RC-REG series appeared to be less noisy and provided more homogeneous ETM parameter values than MOCO and UNREG maps. Distorted registration with MOCO yielded distorted ETM parameters maps as shown in figure 4.

It is noteworthy that two exams had to be discarded from the segment analysis because of a too thin left ventricle myocardial wall, which did not allow for the extraction of a sufficient number of voxels not affected by partial volume effect. This underlines the drawback of low-resolution acquisitions in first-pass protocols. This is a common limitation to all quantitative perfusion methods and developments still have to be made especially for application to patients with dilated cardiomyopathy.

In one case, $T1_0$ map and DCE slices were not acquired in the exact same locations. This exam represents one limitation of our workflow, which requires the $T1_0$ information (DCE baseline) from a separate breath-held acquisition of T1 map. Cernicanu and Axel method [38] for the signal to [CA] conversion could bring a good solution to avoid the use of T1 mapping and its drawbacks. Another point of improvement of our workflow would be to include a better way to measure or correct the AIF which would guarantee a better signal to CA concentration conversion and ultimately a more accurate measure of ETM parameters. There is still no consensus on which method to use but dual bolus [39], [40] or dual sequence [14], [41] methods

are valuable, although imperfect candidates to ensure a more reliable AIF measurement.

4.2 Comparison between ECV_{ETM} and ECV_{T1}

We found a very strong correlation between ETM and T1-based ECV average myocardial values. ECV_{ETM} values exhibited lower absolute values compared to ECV_{T1}. In their study, Kunze et al. [19] also reported both strong correlation between perfusion and ECV_{T1} and lower values for ECV estimated from DCE data. This underestimation was slightly more pronounced in our study. The use of ETM, which is a suitable model only under certain conditions of perfusion and flow in the tissue [42], could explain a sub-optimal estimation of ECV. Although, the presented results, in line with the literature, illustrate the feasibility of ECV measurement using DCE-MRI.

ECV_{ETM} values were able to separate the two groups as distinctly as ECV_{T1} values. One might add that the cutoff ECV value was chosen from the reported values in the literature to discriminate between healthy and pathologic subjects, but this arbitrary separation requires a larger study to confirm its clinical utility..

Between the two ECV measurement methods, the ETM technique is more error prone as more steps are required for the creation of an ECV map. However, the quality of T1-based ECV map is also dependent on the successful registration of the T1 weighted images necessary to reconstruct each T1 map and the registration of both native and post injection T1 maps. Low resolution acquisition needs to be improved to enable a more accurate permeability and ECV quantification using the ETM method, and to avoid partial volume effects in myocardium edge voxels. However, in the context of the characterization of a diffuse pathology like fibrosis

(therefore not located to a specific spot) such low resolution could be sufficient to assess the general state of the myocardial tissue. Furthermore, the low-resolution analysis of the first 2 minutes after injection could help the radiologist to decide whether it worth waiting for a 10 to 15 minutes high-resolution post injection T1 map or even an LGE acquisition. This could therefore be a useful tool to shorten CMR exams and to personalize them to each patient's requirements.

The acquisition duration of at least 2 minutes is enough to guarantee an estimation error of Ve inferior to 5% in healthy myocardium, but could lead to slightly more imprecision in the infarcted area, as demonstrated by Pack et al. [18]. In the same study, they also shown an increase of such error if the acquisition duration is below this limit. According to different studies, the optimal DCE duration ranged from 2 to 5 minutes [18], [42]–[44]. A longer acquisition duration, e.g. 3 minutes, could improve the precision of Ve estimation (and other ETM parameters) and therefore, reduce the wider distribution of ECV_{ETM} values compared to ECV_{T1} ones as reported in figure 6. This wider distribution could also result from the fact that the ECV_{ETM} parameter is obtained from dynamic data. It is therefore more prone to influences of the local perfusion/permeability regime unlike T1-based ECV, estimated at equilibrium.

Despite these limitations, this study demonstrated a clear correlation between compartment parameter estimation from a dynamic perfusion analysis and those measured with the longer static T1-based method. All these results are in agreement with previous related works, but further investigations on a larger population is still needed to fully validate these findings.

5 CONCLUSION:

We presented a complete workflow for the processing of DCE-MRI for compartmental analysis of the myocardial tissue. We were able to demonstrate better registration quality of the presented RC-REG algorithm over the in-line MOCO algorithm. RC-REG algorithm allowed us to compute good quality parametric maps. Resulting ECV_{ETM} parameters exhibited strong correlation with ECV values extracted from MOLLI T1 maps. These results give an additional asset to quantitative cardiac perfusion and permeability MRI in order to assess ECV with a low resolution 2 minutes DCE-MRI acquisition against the current 10-15 minutes T1-based method.

Acknowledgements:

Authors want to acknowledge the work of the radiology technician's team of the Hospital and the help of the vendor's clinical scientist Khalid Ambarki, Ph.D., for its technical help. We also acknowledge J. Oster, Ph.D., for his valuable comments and corrections on the manuscript.

Funding sources:

Results incorporated in this article received funding from the Investments for the Future program under grant agreement: No ANR-15-RHU-0004.

ABBREVIATIONS:

CMR: Cardiac Magnetic Resonance imaging, DCE: Dynamic Contrast Enhancement, ECV: Extracellular volume fraction, EES: Extracellular Extra vascular Space, ETM: Extended Tofts Model, MRI: Magnetic Resonance Imaging, CA: Contrast Agent, RC: Residual Complexity, SD: Standard Deviation, T1w: T1 weighted

REFERENCES:

[1] Flett Andrew S. *et al.*, “Equilibrium Contrast Cardiovascular Magnetic Resonance for the Measurement of Diffuse Myocardial Fibrosis,” *Circulation*, vol. 122, no. 2, pp. 138–144, Jul. 2010, doi: 10.1161/CIRCULATIONAHA.109.930636.

[2] M. Fontana *et al.*, “Comparison of T1 mapping techniques for ECV quantification. Histological validation and reproducibility of ShMOLLI versus multibreath-hold T1 quantification equilibrium contrast CMR,” *J Cardiovasc Magn Reson*, vol. 14, no. 1, p. 88, Dec. 2012, doi: 10.1186/1532-429X-14-88.

[3] R. J. T. Kim, D. J. Shah, and R. M. Judd, “How we perform delayed enhancement imaging.,” *Journal of cardiovascular magnetic resonance : official journal of the Society for Cardiovascular Magnetic Resonance*, vol. 5, no. 3, pp. 505–514, 2003, doi: 10.1081/JCMR-120022267.

[4] M. C. Dulce *et al.*, “MR imaging of the myocardium using nonionic contrast medium: signal-intensity changes in patients with subacute myocardial infarction.,” *American Journal of Roentgenology*, vol. 160, no. 5, pp. 963–970, May 1993, doi: 10.2214/ajr.160.5.8470611.

[5] L. E. J. Thomson, R. J. Kim, and R. M. Judd, “Magnetic resonance imaging for the assessment of myocardial viability,” *Journal of Magnetic Resonance Imaging*, vol. 19, no. 6, pp. 771–788, 2004, doi: 10.1002/jmri.20075.

[6] H. Arheden *et al.*, “Measurement of the Distribution Volume of Gadopentetate Dimeglumine at Echo-planar MR Imaging to Quantify Myocardial Infarction: Comparison with 99mTc-DTPA Autoradiography in Rats,” *Radiology*, vol. 211, no. 3, pp. 698–708, Jun. 1999, doi: 10.1148/radiology.211.3.r99jn41698.

[7] M. Ugander *et al.*, “Extracellular volume imaging by magnetic resonance imaging provides insights into overt and sub-clinical myocardial pathology,” *Eur Heart J*, vol. 33, no. 10, pp. 1268–1278, May 2012, doi: 10.1093/eurheartj/ehr481.

[8] D. R. Messroghli *et al.*, “Clinical recommendations for cardiovascular magnetic resonance mapping of T1, T2, T2* and extracellular volume: A consensus statement by the Society for Cardiovascular Magnetic Resonance (SCMR) endorsed by the European Association for Cardiovascular Imaging (EACVI),” *Journal of Cardiovascular Magnetic Resonance*, vol. 19, no. 1, p. 75, Oct. 2017, doi: 10.1186/s12968-017-0389-8.

[9] P. Croisille, “Imagerie de diffusion cardiaque : vers une nouvelle approche de l’ischémie myocardique ?,” *Journal de Radiologie*, vol. 90, no. 4, pp. 455–457, Apr. 2009, doi: 10.1016/S0221-0363(09)74002-8.

[10] S. Nielles-Vallespin, A. Scott, P. Ferreira, Z. Khalique, D. Pennell, and D. Firmin, “Cardiac Diffusion: Technique and Practical Applications,” *Journal of Magnetic Resonance Imaging*, vol. 52, no. 2, pp. 348–368, 2020, doi: 10.1002/jmri.26912.

[11] N. Wilke *et al.*, “Contrast-enhanced first pass myocardial perfusion imaging: Correlation between myocardial blood flow in dogs at rest and during hyperemia,” *Magnetic Resonance in Medicine*, vol. 29, no. 4, pp. 485–497, 1993, doi: 10.1002/mrm.1910290410.

[12] M. Jerosch-Herold, N. Wilke, A. E. Stillman, and R. F. Wilson, “Magnetic resonance quantification of the myocardial perfusion reserve with a Fermi function model for constrained deconvolution,” *Medical Physics*, vol. 25, no. 1, p. 73, 1998, doi: 10.1118/1.598163.

[13] K. D. Knott *et al.*, “Quantitative myocardial perfusion in coronary artery disease: A perfusion mapping study,” *Journal of Magnetic Resonance Imaging*, vol. 0, no. 0, doi: 10.1002/jmri.26668.

[14] P. Kellman *et al.*, “Myocardial perfusion cardiovascular magnetic resonance: optimized dual sequence and reconstruction for quantification,” *Journal of Cardiovascular Magnetic Resonance*, vol. 19, no. 1, Dec. 2017, doi: 10.1186/s12968-017-0355-5.

[15] J. B. Bassingthwaighte, C. Y. Wang, and I. S. Chan, “Blood-Tissue Exchange via Transport and Transformation by Capillary Endothelial Cells,” *Circ Res*, vol. 65, no. 4, pp. 997–1020, Oct. 1989, Accessed: Mar. 06, 2019. [Online]. Available: https://www.ncbi.nlm.nih.gov/pmc/articles/PMC3454538/.

[16] N. A. Pack and E. V. R. DiBella, “Comparison of myocardial perfusion estimates from dynamic contrast-enhanced magnetic resonance imaging with four quantitative analysis methods,” *Magnetic Resonance in Medicine*, vol. 64, no. 1, pp. 125–137, Jul. 2010, doi: 10.1002/mrm.22282.

[17] H. B. Larsson, T. Fritz-Hansen, E. Rostrup, L. Søndergaard, P. Ring, and O. Henriksen, “Myocardial perfusion modeling using MRI,” *Magnetic Resonance in Medicine*, vol. 35, no. 5, pp. 716–726, 1996, Accessed: Feb. 16, 2017. [Online]. Available: http://onlinelibrary.wiley.com/doi/10.1002/mrm.1910350513/full.

[18] N. A. Pack, E. V. R. DiBella, B. D. Wilson, and C. J. McGann, “Quantitative myocardial distribution volume from dynamic contrast-enhanced MRI,” *Magnetic Resonance Imaging*, vol. 26, no. 4, pp. 532–542, May 2008, doi: 10.1016/j.mri.2007.10.003.

[19] K. P. Kunze *et al.*, “Measurement of extracellular volume and transit time heterogeneity using contrast-enhanced myocardial perfusion MRI in patients after acute myocardial infarction,” *Magnetic Resonance in Medicine*, vol. 77, no. 6, pp. 2320–2330, 2017, doi: 10.1002/mrm.26320.

[20] H. Xue *et al.*, “Unsupervised Inline Analysis of Cardiac Perfusion MRI,” in *Medical Image Computing and Computer-Assisted Intervention – MICCAI 2009*, Berlin, Heidelberg, 2009, pp. 741–749, doi: 10.1007/978-3-642-04271-3_90.

[21] G. Adluru, E. V. R. DiBella, and M. C. Schabel, “Model-based registration for dynamic cardiac perfusion MRI,” *Journal of Magnetic Resonance Imaging*, vol. 24, no. 5, pp. 1062–1070, 2006, doi: 10.1002/jmri.20756.

[22] J. Milles, R. J. van der Geest, M. Jerosch-Herold, J. H. C. Reiber, and B. P. F. Lelieveldt, “Fully Automated Motion Correction in First-Pass Myocardial Perfusion MR Image Sequences,” *IEEE Transactions on Medical Imaging*, vol. 27, no. 11, pp. 1611–1621, Nov. 2008, doi: 10.1109/TMI.2008.928918.

[23] M. Benovoy, M. Jacobs, F. Cheriet, N. Dahdah, A. E. Arai, and L.-Y. Hsu, “A Robust Universal Nonrigid Motion Correction Framework for First-Pass Cardiac Magnetic Resonance Perfusion Imaging,” *J Magn Reson Imaging*, vol. 46, no. 4, pp. 1060–1072, Oct. 2017, doi: 10.1002/jmri.25659.

[24] V. Hamy *et al.*, “Respiratory motion correction in dynamic MRI using robust data decomposition registration – Application to DCE-MRI,” *Medical Image Analysis*, vol. 18, no. 2, pp. 301–313, Feb. 2014, doi: 10.1016/j.media.2013.10.016.

[25] A. Myronenko and X. Song, “Intensity-Based Image Registration by Minimizing Residual Complexity,” *IEEE Transactions on Medical Imaging*, vol. 29, no. 11, pp. 1882–1891, Nov. 2010, doi: 10.1109/TMI.2010.2053043.

[26] Z. Wang, A. C. Bovik, H. R. Sheikh, and E. P. Simoncelli, “Image Quality Assessment: From Error Visibility to Structural Similarity,” *IEEE Trans. on Image Process.*, vol. 13, no. 4, pp. 600–612, Apr. 2004, doi: 10.1109/TIP.2003.819861.

[27] J. C. Moon *et al.*, “Myocardial T1 mapping and extracellular volume quantification: a Society for Cardiovascular Magnetic Resonance (SCMR) and CMR Working Group of the European Society of Cardiology consensus statement,” *Journal of Cardiovascular Magnetic Resonance*, vol. 15, no. 1, p. 92, Oct. 2013, doi: 10.1186/1532-429X-15-92.

[28] null null *et al.*, “Standardized Myocardial Segmentation and Nomenclature for Tomographic Imaging of the Heart,” *Circulation*, vol. 105, no. 4, pp. 539–542, Jan. 2002, doi: 10.1161/hc0402.102975.

[29] A. Sotiras, C. Davatzikos, and N. Paragios, “Deformable Medical Image Registration: A Survey,” *IEEE Transactions on Medical Imaging*, vol. 32, no. 7, pp. 1153–1190, Jul. 2013, doi: 10.1109/TMI.2013.2265603.

[30] A. Menys *et al.*, “Dual registration of abdominal motion for motility assessment in free-breathing data sets acquired using dynamic MRI,” *Phys. Med. Biol.*, vol. 59, no. 16, pp. 4603–4619, Jul. 2014, doi: 10.1088/0031-9155/59/16/4603.

[31] Q. Feng *et al.*, “Liver DCE-MRI Registration in Manifold Space Based on Robust Principal Component Analysis,” *Scientific Reports*, vol. 6, p. 34461, Sep. 2016, doi: 10.1038/srep34461.

[32] C. M. Scannell, A. D. M. Villa, J. Lee, M. Breeuwer, and A. Chiribiri, “Robust Non-Rigid Motion Compensation of Free-Breathing Myocardial Perfusion MRI Data,” *IEEE Transactions on Medical Imaging*, vol. 38, no. 8, pp. 1812–1820, Aug. 2019, doi: 10.1109/TMI.2019.2897044.

[33] M. J. Ledesma-Carbayo, P. Kellman, A. E. Arai, and E. R. McVeigh, “Motion corrected free-breathing delayed-enhancement imaging of myocardial infarction using nonrigid registration,” *Journal of Magnetic Resonance Imaging*, vol. 26, no. 1, pp. 184–190, 2007, doi: 10.1002/jmri.20957.

[34] B. Pontré *et al.*, “An Open Benchmark Challenge for Motion Correction of Myocardial Perfusion MRI,” *IEEE Journal of Biomedical and Health Informatics*, vol. 21, no. 5, pp. 1315–1326, Sep. 2017, doi: 10.1109/JBHI.2016.2597145.

[35] M. Salerno and C. M. Kramer, “Advances in Parametric Mapping With CMR Imaging,” *JACC: Cardiovascular Imaging*, vol. 6, no. 7, pp. 806–822, Jul. 2013, doi: 10.1016/j.jcmg.2013.05.005.

[36] M. Salerno *et al.*, “Recent Advances in Cardiovascular Magnetic Resonance Techniques and Applications,” *Circ Cardiovasc Imaging*, vol. 10, no. 6, Jun. 2017, doi: 10.1161/CIRCIMAGING.116.003951.

[37] R. Zhou *et al.*, “Simple motion correction strategy reduces respiratory-induced motion artifacts for k-t accelerated and compressed-sensing cardiovascular magnetic resonance perfusion imaging,” *Journal of Cardiovascular Magnetic Resonance*, vol. 20, no. 1, p. 6, Feb. 2018, doi: 10.1186/s12968-018-0427-1.

[38] A. Cernicanu and L. Axel, “Theory-Based Signal Calibration with Single-Point T1 Measurements for First-Pass Quantitative Perfusion MRI Studies,” *Academic Radiology*, vol. 13, no. 6, pp. 686–693, Jun. 2006, doi: 10.1016/j.acra.2006.02.040.

[39] T. F. Christian *et al.*, “Absolute Myocardial Perfusion in Canines Measured by Using Dual-Bolus First-Pass MR Imaging,” *Radiology*, vol. 232, no. 3, pp. 677–684, Sep. 2004, doi: 10.1148/radiol.2323030573.

[40] L.-Y. Hsu, K. L. Rhoads, J. E. Holly, P. Kellman, A. H. Aletras, and A. E. Arai, “Quantitative myocardial perfusion analysis with a dual-bolus contrast-enhanced

first-pass MRI technique in humans," *J Magn Reson Imaging*, vol. 23, no. 3, pp. 315–322, Mar. 2006, doi: 10.1002/jmri.20502.

[41] P. D. Gatehouse, A. G. Elkington, N. A. Ablitt, G.-Z. Yang, D. J. Pennell, and D. N. Firmin, "Accurate assessment of the arterial input function during high-dose myocardial perfusion cardiovascular magnetic resonance," *Journal of Magnetic Resonance Imaging*, vol. 20, no. 1, pp. 39–45, Jul. 2004, doi: 10.1002/jmri.20054.

[42] S. P. Sourbron and D. L. Buckley, "On the scope and interpretation of the Tofts models for DCE-MRI," *Magnetic Resonance in Medicine*, vol. 66, no. 3, pp. 735–745, Sep. 2011, doi: 10.1002/mrm.22861.

[43] F. Khalifa *et al.*, "Models and methods for analyzing DCE-MRI: A review," *Medical Physics*, vol. 41, no. 12, p. 124301, Dec. 2014, doi: 10.1118/1.4898202.

[44] P. S. Tofts, "T1-weighted DCE Imaging Concepts: Modelling, Acquisition and Analysis," p. 5.

FIGURES AND LEGENDS:

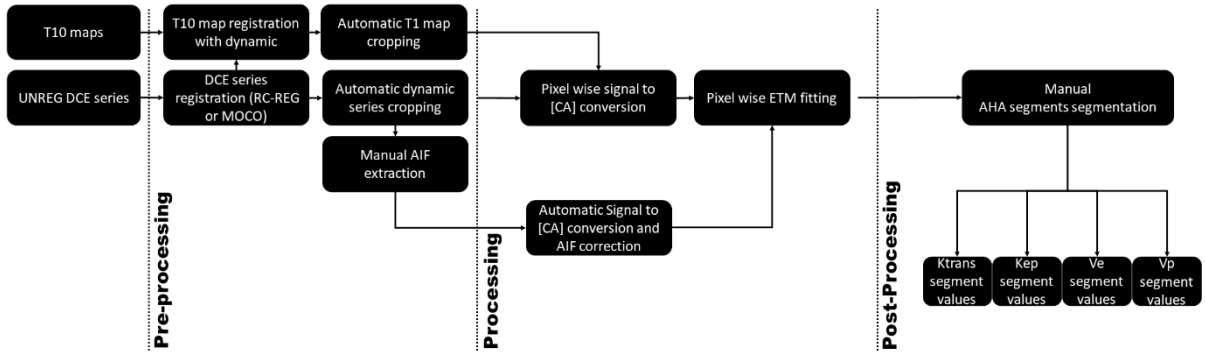

Figure 1: Framework diagram. The framework is split in 3 major parts: 1) pre-processing consisting in preparing the necessary data for the processing part; 2) processing consisting in signal to CA concentration conversion of every pixel from DCE series, AIF correction and ETM calculation which yields to the processing of the four permeability maps; and 3) the post-processing part, consisting in the extraction of the permeability maps parameters with American Heart Association segments.

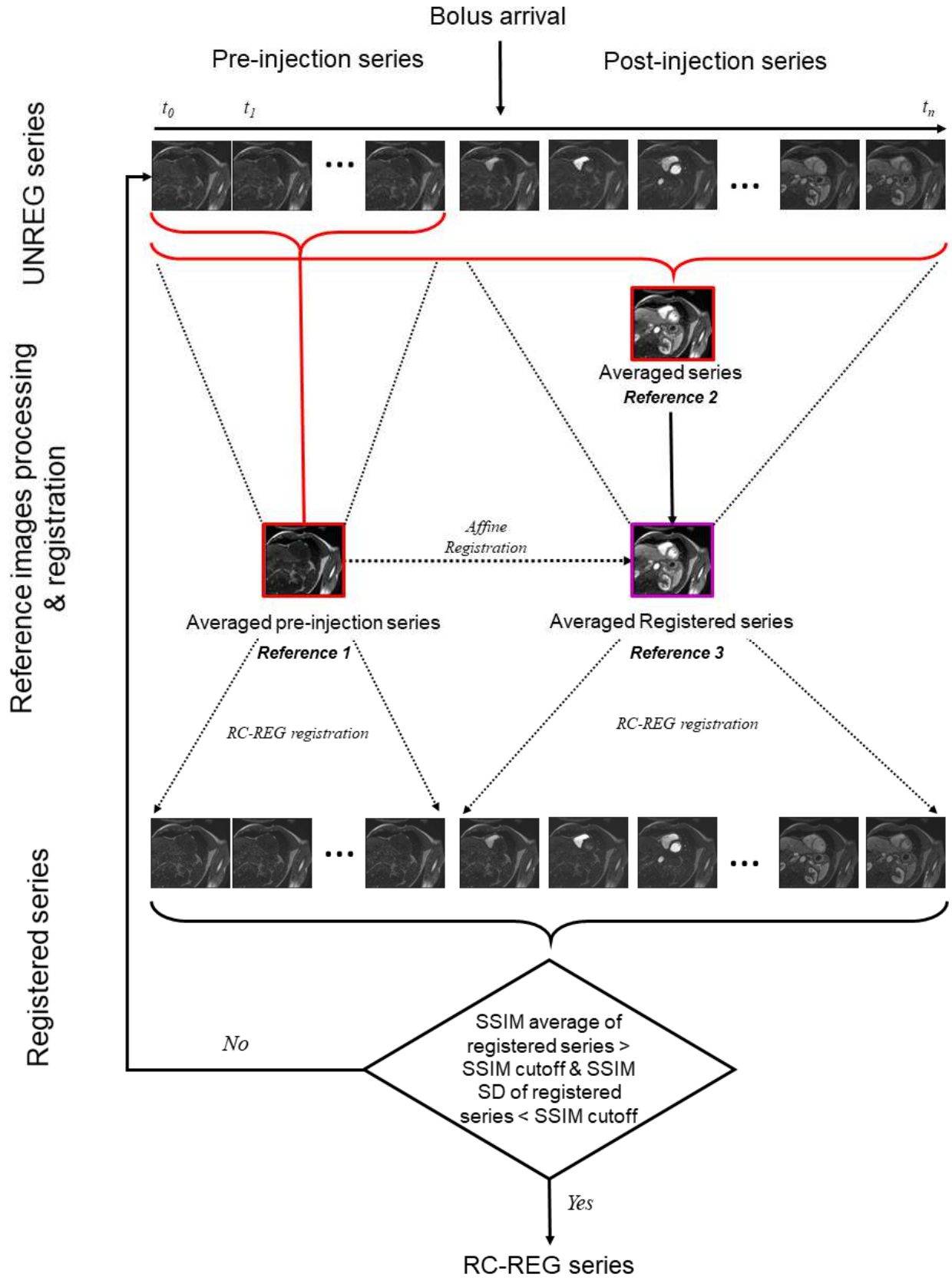
Bolus arrival
Pre-injection series
Post-injection series
t_0
t_1
t_n
UNREG series
Reference images processing & registration
Averaged series
Reference 2
Affine Registration
Averaged pre-injection series
Reference 1
Averaged Registered series
Reference 3
RC-REG registration
RC-REG registration
Registered series
No
SSIM average of registered series > SSIM cutoff & SSIM SD of registered series < SSIM cutoff
Yes
RC-REG series

1

Figure 2: RC-REG algorithm diagram. The algorithm is based on the determination of two reference images to register pre-injection series and post-injection series images. Once the series is registered, the SSIM average and SD values of the series are compared to SSIM cutoff values (0.81 and 0.028 respectively). The algorithm iterates until these two conditions are fulfilled.

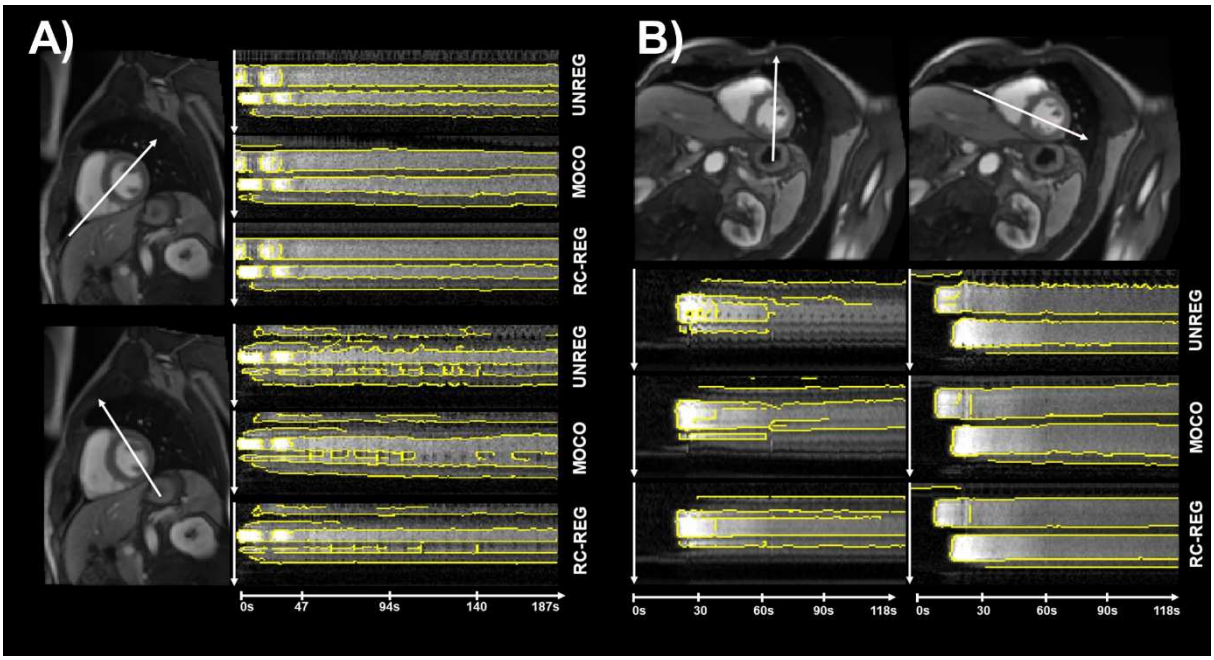

Figure 3: Example of two slice profiles from two exams with different acquisition orientation. Intensity based edges detection (canny filter) have been applied on the line profiles images and are highlighted in yellow. It was used to emphasize both the registration quality of RC-REG and distortion induced by the MOCO algorithm. A. First exam slice profiles. It shows on both profiles important distortions brought by the MOCO algorithm, especially after the first pass. RC-REG series of both slice profiles does not present distortion such MOCO one. Although we noted a very slight distortion of the anterior segments on the first slice during the first-pass. B. This second example shows similar results with A on a different acquisition orientation. While both MOCO and RC-REG series present a suitable respiratory motion correction, MOCO series are polluted with blatant distortion over the whole profiles which are not encountered on RC-REG series.

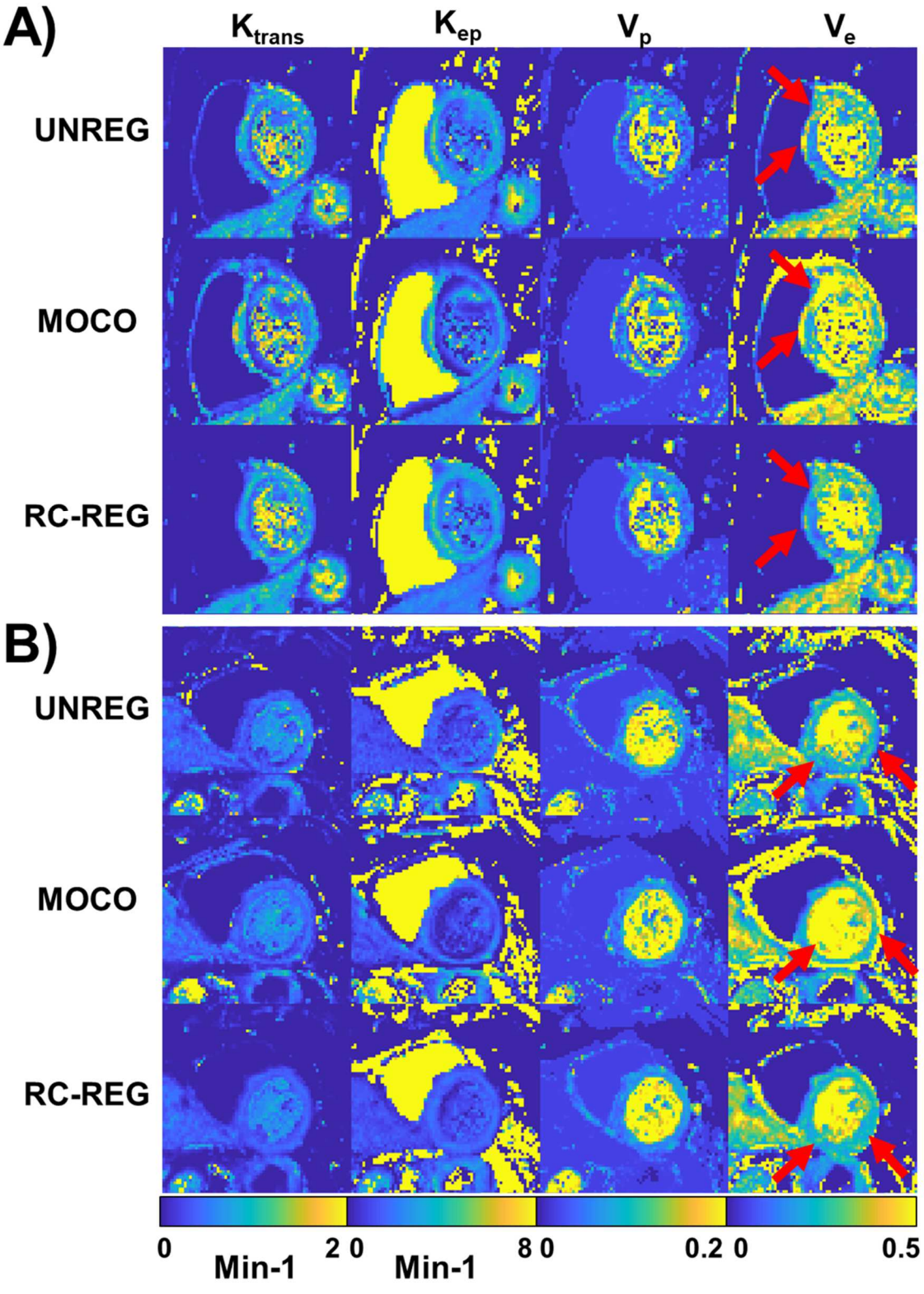
A)
K_{trans}
K_{ep}
V_p
V_e
UNREG
MOCO
RC-REG
B)
UNREG
MOCO
RC-REG
0
2 0
Min-1
8 0
Min-1
0.2 0
0.5

1

Figure 4: Example of two sets of permeability parameters. A and B sets were extracted from UNREG, MOCO and RC-REG DCE data. We can observe a better homogeneity of all parameters values on all maps for RC-REG maps compare to others maps. A. Arrows in Ve maps indicates area were RC-REG map substantial homogenization of Ve values. Two areas in the septal segment seemed to be elevated compare to the rest of the myocardium in UNREG and MOCO Ve maps while values appear to be more homogeneous in RC-REG Ve map. B. Arrows in the inferior segment shows much more noise on UNREG Ve map than on RC-REG Ve map while MOCO Ve map seem to be affected by major distortion of the LV.

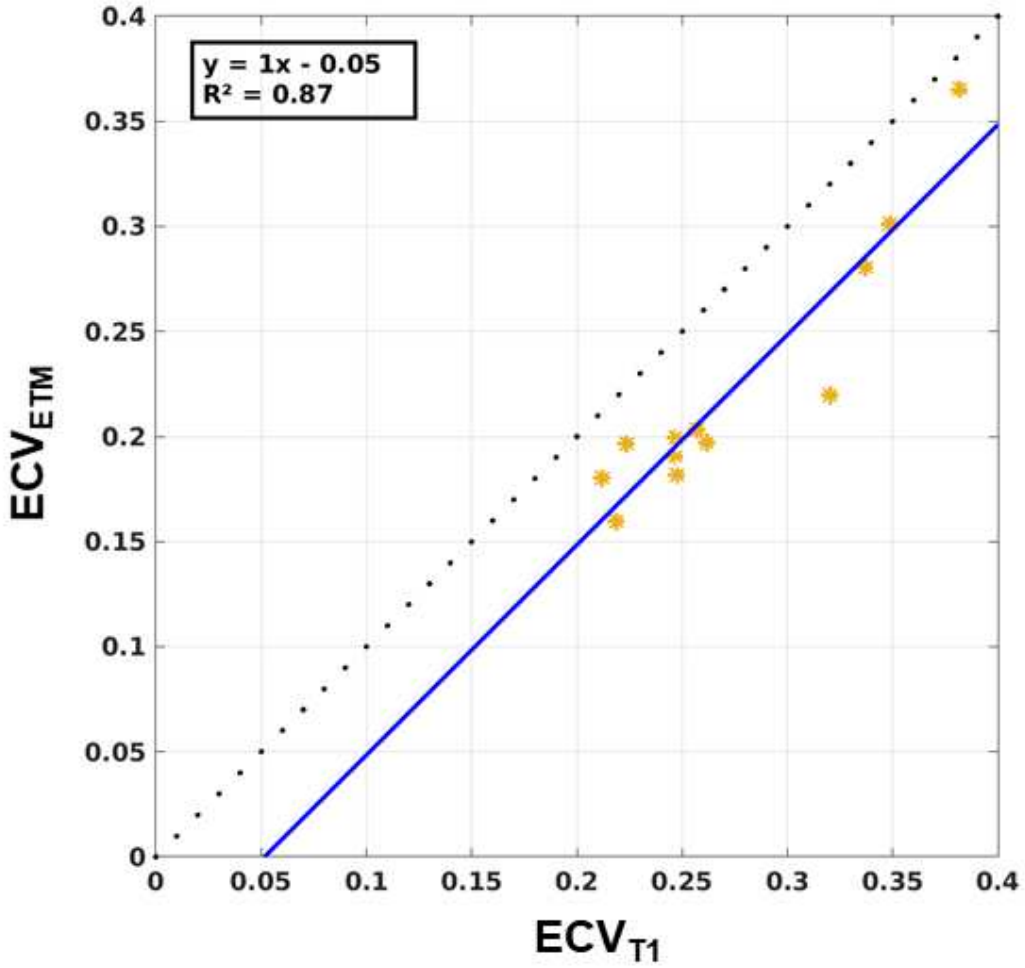

Figure 5: ECV_{ETM} and ECV_{T1} myocardial mean values correlation. The RC-REG ECV_{ETM} values yielded to a very high correlation factor with ECV_{T1} ones ($R^2 = 0.87$) with unity slope. A slight offset equals to -0.05 was nevertheless observed.

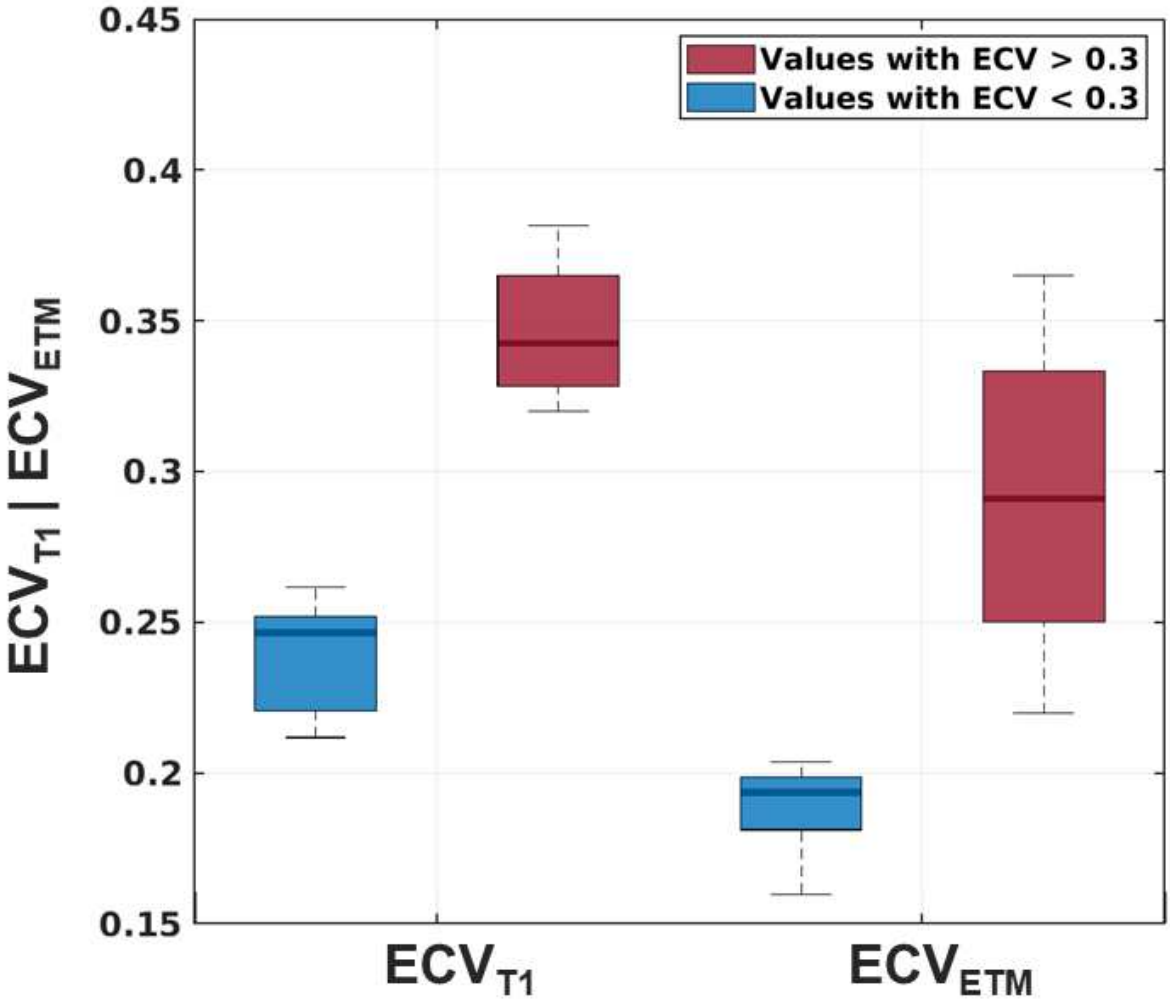

Figure 6: Boxplot of distribution of ECV_{ETM} values corresponding to ECV_{T1} above and below the cutoff value set to 0.3; ECV_{T1} boxplot is given as reference. Permutation test indicated a significant mean difference between the subgroup above (n = 4) and the subgroup below (n = 8) the cutoff value for ECV_{ETM} values.